Lawrence Berkeley National Laboratory
LBL Publications

Title

Feedbacks between hydrological heterogeneity and bioremediation induced biogeochemical transformations

Permalink

https://escholarship.org/uc/item/2pp4c217

Authors

Englert, A.
Hubbard, S.S.
Williams, K.H.
et al.

Publication Date

2009-06-01

eScholarship.org Powered by the California Digital Library
University of California

Feedbacks Between Hydrological Heterogeneity and Bioremediation Induced Biogeochemical Transformations

A. Englert[12], S.S. Hubbard[1], K.H. Williams[1], L. Li[1], C.I. Steefel[1]

[1]Earth Sciences Division, Lawrence Berkeley National Laboratory

[2]now at Bochum University, Applied Geology Department

May 22, 2009

Abstract

For guiding optimal design and interpretation of in-situ treatments that strongly perturb subsurface systems, knowledge about the spatial and temporal patterns of mass transport and reaction intensities are important. Here, a procedure was developed and applied to time-lapse concentrations of a conservative tracer (bromide), an injected amendment (acetate) and reactive species (iron(II), uranium(VI) and sulfate) associated with two field scale biostimulation experiments, which were conducted successively at the same field location over two years. The procedure is based on a temporal moment analysis approach that relies on a streamtube approximation. The study shows that biostimulated reactions can be considerably influenced by subsurface hydrological and geochemical heterogeneities: the delivery of bromide and acetate and the intensity of the sulfate reduction is interpreted to be predominantly driven by the hydrological heterogeneity, while the intensity of the iron reduction is interpreted to be primarily controlled by the geochemical heterogeneity. The intensity of the uranium(VI) reduction appears to be impacted by both the hydrological and geochemical heterogeneity. Finally, the study documents the existence of feedbacks between hydrological heterogeneity and remediation-induced biogeochemical transformations at the field scale, particularly the development of precipitates that may cause clogging and flow rerouting.

Introduction

Biostimulation involves the injection of amendments into the subsurface to encourage in-situ bacteria to degrade or transform contaminants to a less harmful or less mobile state (*1*). Although conceptually simple, biostimulation efficacy can be influenced by the ability to distribute injected amendment through the contaminated region and to maintain favorable hydrobiogeochemical conditions. In practice, ensurance of these conditions can be challenging, since natural variations in subsurface hydrological and biogeochemical properties exist that influence the location and magnitude of the induced reactions (*2*, *3*).

Bioclogging, intensively studied over the last 20 years (*4*), has potential to further impact bioremediation efforts. Examples of biostimulation induced end-products include precipitates, gases, or biomass. As these products accumulate, the potential of clogging the pore space or throats arises. If significant enough, these physical changes in the subsurface system can alter flow and transport characteristics, which in turn have the potential to influence where subsequent injected amendment can be delivered and where biogeochemical transformations occur. Such changes in flow and transport characteristics due to the formation of reaction end products are well studied and documented for laboratory scale experiments (*5*, *6*) and through synthetic experiments (*7*, *8*), but are largely unstudied at the field scale (*4*). Only a few studies have been performed that have documented field scale transformations associated with biostimulation. For example in advance of and during a biostimulation experiment performed at a DOE uranium(VI)-contaminated aquifer in Oak Ridge, TN, a forced gradient tracer test was performed (*9*). Bromide breakthrough curves associated with these tests revealed different responses as a function of time. Similarly, bromide breakthrough data collected in association with a chromium(VI) biostimulation study at the DOE Hanford 100H site revealed different responses as a function of time (*10*). Although these studies suggest that the borehole or aquifer conditions were altered by the biostimulation treatments, the datasets were neither analyzed to assess the spatiotemporal changes in flowpaths or reaction product distributions nor used to assess field-scale feedbacks.

Here, we explore time-lapse solute concentrations of injected amendments, reactants and end-products associated with two field scale biostimulation experiments that were successively conducted

in 2002 and 2003 within a single experimental setup at the Department of Energy (DOE) Integrated Field Research Challenge Site (IFRC) at Rifle, Colorado. The ongoing work within the DOE U(VI)-contaminated aquifer at the Rifle IFRC site focuses on investigating the efficacy of biostimulation for facilitating microbial reduction of U(VI) to U(IV) through injection of acetate as electron donor. Previous research demonstrated that in some monitoring wells, the decline of U(VI) concentrations to below MCL in as little as nine days (*11*, *12*). Two dimensional reactive transport models, developed for the Rifle IFRC site (*13*), have been used to synthetically explore the effects of physical and chemical heterogeneities on the transformation of mineral phases and spatial patterns of biomass accumulation. Simulations from these models suggest that the volume of the evolved iron sulfides, calcite and biomass can total up to 5.5 % of the pore space (*14*).

The aim of the present study is to analyze the time-lapse solute concentrations, acquired during the 2002 and 2003 biostimulation experiments at the Rifle IFRC site, to characterize the spatial distributions of bromide, acetate amendment, and reaction products at the field scale. With this information, we explore the dependencies of reactive species on amendment delivery and their change over time. To meet this objective, we draw in principle on the temporal moment analysis of locally measured bromide breakthrough curves (*15*, *16*) and previously developed streamtube approach for representing flow and transport through a transect perpendicular to the mean flow direction (*17*, *18*). However, we extend these approaches to estimate the accumulated response of the complex subsurface as a function of the injection of amendments. We utilize the new approach to gain insights about the interactions between subsurface heterogeneity and non-reactive as well as reactive transport. This understanding is expected to be helpful for guiding the design of in-situ subsurface manipulations, such as those used to remediate contaminants, enhance oil recovery and sequester carbon dioxide.

In the following sections, we describe the procedure for the estimation of accumulated responses of conservative and reactive species as function of the injection and heterogeneity. We apply the procedure to bromide, acetate, iron, uranium and sulfate measurements collected during the 2002 and 2003 biostimulation experiments at the Rifle IFRC site. We then compare the spatial patterns of accumulated responses and their changes over time. The present study is, to our knowledge, the first systematic analysis of time-lapse concentration data to assess field-scale feedbacks associated

with a biostimulation field experiment.

Materials and Methods

In the following section we first describe the general setup of the field biostimulation experiments and the biogeochemical reaction network. We present then a moment based approach to analyze the time-lapse concentrations of conservative and reactive species to estimate the spatial distribution of velocities and accumulated responses as function of the injection and the subsurface heterogeneity.

Experimental Design

Our study focuses on experiments collected within the 2002/2003 experiment (Figure 1) at the Rifle IFRC site. The subsurface hydrogeology germane to the biostimulation experiments at the Rifle

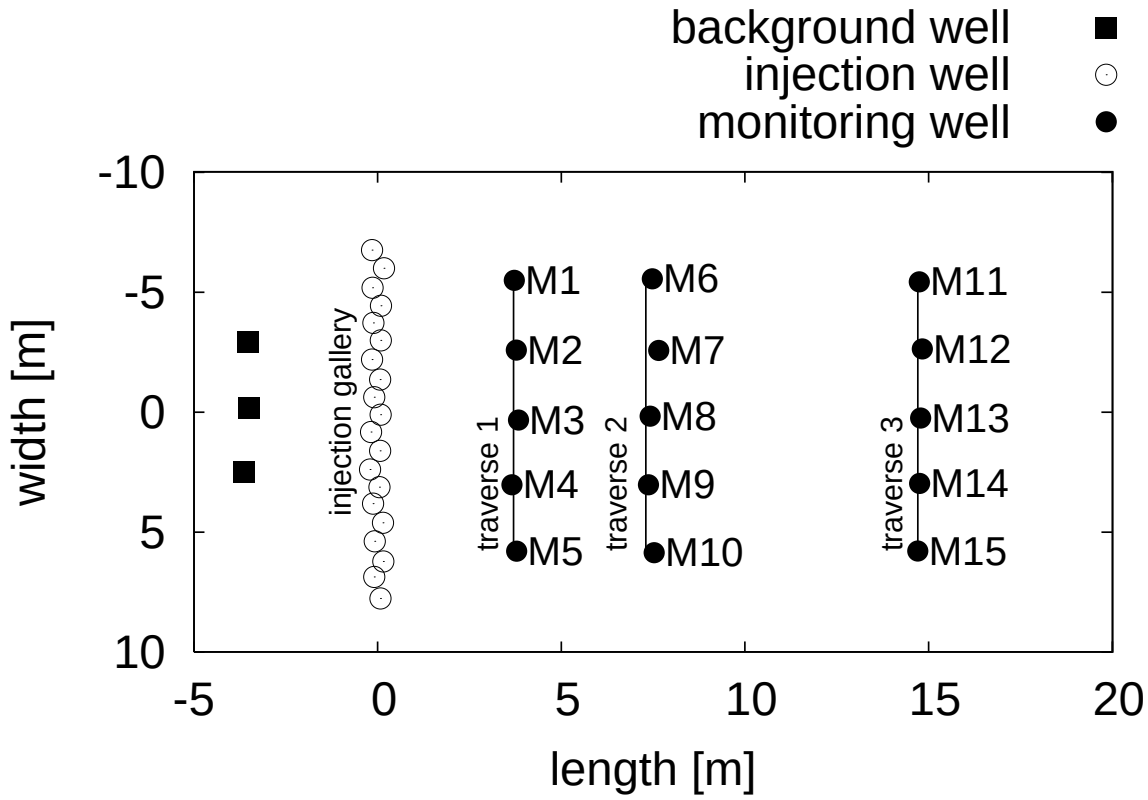

Figure 1: Planview geometry of the 2002/2003 experiment at the Rifle IFRC site. Mean flow direction is roughly from left to right.

IFRC site can be divided into three units. The deeper unit is an Eocene floodplain deposit called

the Wasatch formation, which consists of silty shales of low permeability. At a depth of ∼6.25 m below ground surface, the Wasatch formation is overlain by a ∼4.5 m thick alluvial formation of Quaternary age that includes sandy gravely unconsolidated sediments with variable clay content. The shallowest unit is about ∼1.75 m thick and consists of a heterogeneous artificial fill of silty sandy sediments that includes a variable content of gravel and clay (*11*, *12*). The water table (about 5 m below surface), located in the alluvial formation, represents the top of the shallow unconfined alluvial aquifer within which the biostimulation experiments were performed. The aquifers' average porosity was 0.27 (*11*). Annual changes in precipitation, snowfall, and snow-melt govern the recharge of the watershed. This results in annual groundwater level variations up to ∼1.2 m at the Rifle IFRC site. In the two experiments, the average hydraulic gradients were similar (2002: 0.0039 m/m, 2003: 0.0036 m/m) and roughly aligned with the long axis of the experiment (average deviation from long axis direction in 2002: 15 $^\circ$, 2003: 13 $^\circ$). Results of detailed analysis of the gradients are provided in the supplementary information (Figures SI-2-SI-4).

Utilized within the experiment were 3 upgradient wells, 20 injection wells, and 15 downgradient monitoring wells aligned over three rows (Figure 1). These wells (inner diameter 5.08 cm) were installed to a depth of 6.1 m and were screened along the entire saturated zone of interest from 1.5 m to 6.1 m (*11*, *12*). At the injection wells, the co-injected bromide (∼84 mol 2002 and 2003) and acetate (∼881 mol in 2002 and ∼2822 mol in 2003) was mixed with ∼8500 l of on site water from an upstream well in both experiments. During both experiments, this was accomplished by filling a stainless steel tank (2120 l) four times with the on-site water and adding each time $\sim \frac{1}{4}$ of the total amount of bromide and acetate. From the tank, the bromide and acetate amended water was injected into the the subsurface through the injection gallery. Here, each injection well was equipped with three injection ports, positioned at three different depth in the saturated zone. At each of the injection ports the prepared water was injected with an injection rate of $\sim 1.2\ l/d$ over ∼100 days. Resulting bromide and acetate concentrations in the vicinity of the injection gallery was impacted by variations in the water level, the injection concentration, and the injection rate; field notes were used to estimate injection functions for the experiments (for details see Figure SI-5). Before, during and after both experiments, the background and the monitoring wells were used to sample the groundwater over 260 days in 2002 and 220 days in 2003. Sampling of groundwater was

performed in two steps. First, about 12 l groundwater were purged from the center of the water-column using a peristaltic pump until pH, dissolved oxygen, conductivity and redox potential (all measured on surface with a multi-probe data sonde) stabilized. Second, the samples were collected with the same pumping equipment as during the purging procedure (*11*). Thereafter, groundwater samples were used to monitor solute concentrations of acetate, bromide, iron(II), uranium(VI) and sulfate (*11*, *12*).

Biogeochemical Reaction Network

The experiments conducted in 2002 and 2003 both included a coinjection of acetate and bromide over a three-month period. The biogeochemical reaction network associated with these stimulations were developed using field and column data after (*13*, *14*). Iron reduction is expected to occur first, reducing iron (hydro)oxide (represented by FeOOH(s) in Figure SI-6) to ferrous iron (Fe(II)) by iron reducing bacteria (*Geobacter* species, common in the Rifle subsurface). The iron reducer is expected to reduce aqueous U(VI) to immobile U(IV). After the depletion of "bioavailable" iron, sulfate is expected to be reduced by sulfate reducers (sulfate reducing proteobacteria), which should lead to the accumulation of aqueous S(−II) and eventually the formation of amorphous FeS(am) (*11*, *12*). These biogeochemical reactions also produce bicarbonate, which can react with Ca^{2+} and Fe^{2+} species in the groundwater to produce precipitates, such as calcite ($CaCO_3$) and siderite ($FeCO_3$) (*14*). Figure SI-6 shows several major microbially-mediated reactions and the associated mineral dissolution/precipitation reactions. A complete reaction network would also include surface complexation and aqueous speciation reactions.

Analysis of Transport in a Bundle of Streamtubes

In order to assess the spatiotemporal distributions of measured solutes in a naturally complex subsurface system, methods are needed to characterize multidimensional flow and transport in terms of meaningful parameters, often based on limited field observations. To meet this objective, we represent transport as a bundle of one dimensional convective dispersive processes along an imaginary bundle of streamtubes (*17–21*). With this representation, flow and transport characteristics (for

example, the pore velocity) are integrated over the distance between injection and observation well, rather than being a measure of a localized property. To distinguish the integrated transport characteristics from localized properties, we refer to the former as "apparent". As such, these apparent transport characteristics may change with distance from the injection, since the averaging volume of these apparent parameters changes with distance. As a consequence of the aquifer's heterogeneity, they may also differ between different locations, even though the locations are equidistant from the injection. In this framework, a single bromide breakthrough curve represents the apparent result of a conservative transport process along a single streamtube. The spatial variability of the apparent transport characteristics can be assessed through analyzing several breakthrough curves from different observation wells along a traverse perpendicular to the mean flow direction. The temporal variability of apparent transport parameters can be assessed by analyzing consecutive experiments.

To estimate apparent parameters based on bromide breakthrough curves, we perform a temporal moment analysis (*15*). We expand the streamtube representation combined with temporal moment analysis in terms of an apparent accumulated mass, which is a flexible and quantitative estimate of the total amount of amendment delivered to a given monitoring location and the total amount of reactants and products, delivered after formation or consumption as result of biogeochemical reactions between injection and monitoring location. The apparent accumulated mass is based on the measure of the previously-defined accumulated mass (*16*), but is modified here to allow for the quantitative characterization of conservative and reactive species in the framework of a streamtube approach. In the following, we first introduce the procedure to estimate temporal moments and the apparent velocity at a given location in the presence of a complex injection function. We subsequently describe the estimation of the apparent accumulated mass.

Temporal Moment Analysis and Apparent Velocity Estimation

To estimate the zeroth temporal moment (t_0) (the area under a breakthrough curve) of bromide and acetate at each monitoring well we use a traditional approach:

$$t_0(x) \;=\; \int_0^\infty C(x,t)\,dt, \tag{1}$$

where C is the solute concentration, x is the position in space and t is the time. For example, the zeroth temporal moment of the bromide and acetate breakthrough curves at well M08 during the 2003 experiment are shown in pink in Figures SI-1c and SI-1d, respectively.

To estimate the zeroth temporal moment of iron(II), uranium(VI) and sulfate we used

$$t_0(x) \quad = \quad \left| \int_0^\infty C(x,t) - C_b(x,t)\, dt \right|, \tag{2}$$

where C_b is the average background concentration, which was estimated based on the averaged measurements from the three upgradient background wells at each time step (Figure 1). The zeroth moments of iron(II), uranium(VI) and sulfate for the monitoring well M08 in the 2003 experiment are highlighted in pink in Figures SI-1e-g. The calculation of the zeroth moment based on Equation 2 can either quantify reaction products with increased concentrations compared to a background concentration (as in the case of Fe(II)) or reactants with decreased concentrations (as in the cases of U(VI) and sulfate). It is important to note that the estimate of t_0 based on Equation 2 is only valid if the injected water has a concentration similar to the background concentration C_b, as in the case of the Rifle experiments. Furthermore, the estimate of t_0 based on Equation 2 is only valid if the variation of the background concentration is small compared to the concentrations observed at a monitoring well and/or the duration of the experiment is long compared to the mean traveltime from the injection to the monitoring well.

To estimate the apparent velocity, we then calculated the first temporal moment (t_1) of the bromide breakthrough curve, which is identical to the mean arrival time (μ_t) of bromide, following:

$$t_1(x) = \mu_t(x) = \int_0^\infty t \frac{C(x,t)}{t_0}\, dt. \tag{3}$$

For a Dirac pulse, the bromide travel time mean can be used to estimate v_a using a traditional approach ($v_a = \frac{d(x)}{\mu_t(x)}$). However, in our case of a multi-step pulse injection (e.g. Figure SI-1a,b and SI-5), it was necessary to take into account the first moment of the injection function in the estimation of v_a. To do this, we first estimated the first temporal moment of the injection function at the injection gallery ($\mu_{t,INJ}$) and of the bromide breakthrough curves ($\mu_{t,BTC}$) using equations 1

and 3. We then calculated the difference between the mean of the injection time and the mean of the travel time, $\mu_{t,step}$ for every bromide breakthrough dataset:

$$\mu_{t,step}(x) = \mu_{t,BTC}(x) - \mu_{t,INJ}, \tag{4}$$

We then calculated the apparent velocity over a distance, d, from the injection gallery to a given monitoring well by

$$v_a(x) = \frac{d(x)}{\mu_{t,step}(x)}. \tag{5}$$

Apparent Mass Estimation

Previously published research (*16*) has described an accumulated mass ($m_{(acc)}$) concept, which is an integrated measure of mass flux over time at a particular location. With this approach (*16*), the accumulated mass is calculated by taking the product of the zeroth temporal moment of a breakthrough curve and the local groundwater flux (Q) at a position in space ($m_{(acc)} = Q \cdot t_0$). This approach was previously applied to synthetic transport experiments (*16*), where the groundwater flux was known at every position in space. Although a valuable concept, this approach is difficult to apply to field datasets because the local groundwater flux is typically not known. However, if variations of the flow field in time are small during an experiment (as is the case at Rifle: Figures SI-2-SI-5), we can estimate a zeroth moment and apparent velocity at locations where a breakthrough curve of a conservative tracer is measured. Based on these estimates, we can derive an apparent accumulated mass (m_a), or the accumulated mass per pore area integrated over a streamtube from the injection location to a given monitoring well. Synthetic studies of inert tracers have shown that the spatial velocity field is important for estimating the spatiotemporal distribution of solutes at cross-sections perpendicular of the mean velocity (*22*, *23*). These studies have also shown that the usage of the apparent velocity as a proxy for the local velocity can improve estimation of mass fluxes based on resident concentrations measured at monitoring wells during tracer experiments.

Here, we relate the groundwater flux, Q to the local pore velocity, v_p, by $v_p = \frac{Q}{A \cdot \phi}$, where A is the cross-sectional area and ϕ is the porosity of the porous medium through which the groundwater

travels. We can then calculate the accumulated mass (*16*) as $m_{(acc)} = v_p \cdot A \cdot \phi \cdot t_0$. Normalizing the accumulated mass by the porosity and the cross-sectional area, we define the accumulated mass per pore space (m_p) as:

$$m_p(x) = \frac{m_{(acc)}(x)}{A(x) \cdot \phi(x)} \quad (6)$$

$$= v_p(x) \cdot t_0(x). \quad (7)$$

At an injection location, the accumulated mass per pore space can be estimated using Equation 6, where the known total injected mass of a substance is $m_{(acc)}$, the area of injection is $A(x)$ (in our case the length times the height of the injection gallery) and the porosity at the injection is $\phi(x)$. At monitoring wells, where $m_{(acc)}$ is not known, one can instead utilize the apparent velocity (using equations 1, 3, 4 and 5) to estimate the apparent accumulated mass, m_a as:

$$m_a(x) = v_a(x) \cdot t_0(x). \quad (8)$$

As with the apparent velocity, the apparent accumulated mass is also an integrated measure, since both the apparent velocity and the zeroth moment are a result of integrating processes along a streamtube from the injection to the point of monitoring. The apparent accumulated mass is an estimate of the total integrated mass passing an area A within a medium of porosity ϕ during an experiment; its units are mass per area, and we refer to it in from here on as apparent mass ($m_a[\frac{mol}{m^2}]$).

To extend the concept of the apparent mass to reactive species, the approach must consider the nature of the species (i.e., conservative or not, injected or not, reactant or product). However, estimation of the apparent mass is straightforward (using equation 8) once the zeroth temporal moment of the species and the collocated apparent velocity of the conservative tracer are calculated by equations 1-5. For example, the apparent mass of bromide at a given location can be estimated by ($m_a^{bromide}(x) = t_0^{bromide}(x) \cdot v_a^{bromide}(x)$) and the apparent mass of reduced sulfate can be estimated by ($m_a^{sulfate}(x) = t_0^{sulfate}(x) \cdot v_a^{bromide}(x)$). The measure of the apparent mass of the coinjected species bromide and acetate also permits an estimate of the acetate's apparent consumption along

a streamtube:

$$m_a^{consumed\ \ acetate}(x) = \frac{m_p^{injected\ \ acetate}}{m_p^{injected\ \ bromide}} \cdot m_a^{bromide}(x) - m_a^{acetate}(x). \tag{9}$$

where m_p for acetate and bromide can be estimated using Equation 6 and m_a(x) can be estimated for acetate and bromide at monitoring wells using Equation 8.

Results

For both biostimulation experiments, the application of the temporal moment analysis (Equations 1 and 3-4) to the time-lapse monitoring well bromide concentration data and to the estimated bromide injection function (at the injection gallery) permitted an estimate of the apparent velocity (Equation 5) for all monitoring wells, except M10 and M15. The data from the two latter monitoring wells only allowed rough estimates, due to low/no bromide delivery at those locations. The zeroth temporal moments of the injected species (bromide and acetate, calculated using Equation 1) and of other species (reduced uranium(VI), iron(II) and sulfate, calculated using Equation 2) were used in Equation 8 to estimate apparent masses (m_a) for the same monitoring wells. Utilizing Equation 6, we then estimated the accumulated mass of the acetate and bromide injection based on the known measures of the cross-sectional area of the injection gallery, the porosity of the aquifer and injected bromide and acetate masses during the two experiments. Based on acetate and bromide accumulated mass per pore space (m_p) at the injection gallery together with m_a of acetate and bromide at monitoring wells, we estimated the m_a of consumed acetate using Equation 9. As outlined in the prior sections, m_a can be a quantitative measure of both the accumulated appearance or disappearance of a substance. In the following, m_a, calculated based on aqueous concentration data, quantifies on the one hand the appearance of bromide, and reduced Fe(II), and on the other hand the accumulated disappearance of acetate through consumption and U(VI) and sulfate through reduction.

Both the mean of m_a ($\mu(m_a)$) and the standard deviation of m_a ($\sigma(m_a)$) within a control plane are shown in Figure 2 for the two experiments as a function of distance from the injection gallery.

At the injection gallery (distance 0), we utilized m_p as a proxy for m_a of the injected species, bromide and acetate. The m_a of the consumed acetate, and other reactive species (reduced Fe(II), U(VI), and Sulfate) were assumed to be zero at the injection gallery, since no biostimulation was performed upgradient the injection. At the downgradient traverses, $\mu(m_a)$ and $\sigma(m_a)$ are estimated by m_a values at M01-M05 (traverse 1), M06-M09 (traverse 2) and M11-M14 (traverse 3). Figure 2 is discussed in the following, while statistical analysis associated in the interpretation can be found in Tables SI-2-SI-3.

Figure 2a shows the evolution of the $\mu(m_a)$ of bromide as function of distance from the injection gallery. As bromide is inert, Figure 2a illustrates the overall conservative mass transport characteristics during the two biostimulation experiments. Variations in $\mu(m_a)$ of bromide between traverses in both experiments indicate the hydrological heterogeneity of the subsurface, which is only roughly captured by five monitoring wells per traverse. For the bromide data, the ratio between $\mu(m_a)$ at the injection gallery and $\mu(m_a)$ at traverses expresses the estimated mass recovery during the experiments. Mass recovery (not shown) was $\sim$60% at the first, $\sim$100% at the second and $\sim$75% at the third traverse. Figure 2a also shows that $\sigma(m_a)$ is substantial in both experiments, especially along the second traverse. The values of $\mu(m_a)$ and $\sigma(m_a)$ of bromide were similar in the 2003 experiment compared to the 2002 experiment.

The $\mu(m_a)$ of consumed acetate shows significantly higher values in the 2003 experiment compared to the 2002 experiment, which is a consequence of the (three times) higher acetate concentration used during the 2003 injection (Figure 2b). During both experiments, $\mu(m_a)$ of consumed acetate increases with distance to the injection gallery until the second traverse. Further downgradient, $\mu(m_a)$ of consumed acetate decreases slightly. The behavior of $\mu(m_a)$ of consumed acetate is interpreted to be due to a combined effect of acetate consumption and the variability in the mass recovery. The rapid increase of $\mu(m_a)$ of consumed acetate between the injection and the second traverse indicates that most acetate is consumed closer to the injection, which is consistent with reactive model simulations (*14*).

Figure 2c shows that the $\mu(m_a)$ of reduced iron increases with distance to the injection in both experiments and that the variabilities of m_a of Fe(II) ($\sigma(m_a)$) are high. The $\mu(m_a)$ of Fe(II) is similar or slightly smaller in the 2003 experiment compared to the 2002 experiment. We interpret

this result to be associated with the bioavailability of FE(III), which limits iron reduction, although acetate delivery tripled. During both experiments, the $\mu(m_a)$ of reduced sulfate increases between the injection and the first traverse (Figure 2d). The $\mu(m_a)$ of reduced sulfate further increases significantly between the first and second traverse in 2003, before it decreases between the second and third traverse. In 2002, the $\mu(m_a)$ of reduced sulfate reaches a plateau between the second and third traverse, before it decreases slightly towards the third traverse. The $\mu(m_a)$ of reduced sulfate was distinctly higher in the 2003 experiment compared to the 2002 experiment, which we interpret to be due to the higher acetate delivery to the subsurface in 2003. In both experiments, we interpret the decrease of $\mu(m_a)$ of reduced sulfate at further downgradient traverses to be a result of reduced mass recovery. The $\mu(m_a)$ of reduced uranium increases with distance until the second traverse in both experiments (Figure 2d). Between the second and third traverse, $\mu(m_a)$ of reduced uranium increased slightly in 2002, but decreased in 2003. We interpret the decrease in 2003 and the only slight increase in 2002 to be a result of reduced mass recovery. The $\mu(m_a)$ of reduced uranium is higher in the 2003 experiment compared to the 2002 experiment at all traverses. Although we have not yet understood the biogeochemical mechanisms, we speculate this to be a result of the higher acetate delivery in the 2003 experiment.

To explore the spatial patterns of mass transport and biogeochemical end-products, individual m_a values were normalized along traverses. We normalized m_a to extract the spatial behavior of m_a from the overall mass transport behavior (mass recovery) and to compare the spatial patterns of m_a associated with different species, whose m_a were of different orders of magnitude before the normalization procedure. For normalizing the individual m_a at monitoring locations along a given traverse we used $m_a^{norm} = \frac{m_a - \mu(m_a)}{\sigma(m_a)}$. This procedure was carried out for each local m_a value using $\mu(m_a)$ and $\sigma(m_a)$ of the shared traverse. The m_a^{norm} were then linearly spatially interpolated to yield the images shown in Figure 3. In the following, we analyze and interpret the (dis)similarity in the patterns qualitatively using Figure 3 and quantitatively by using associated correlation coefficient (r) (summary of the correlation coefficients given in Table SI-1)

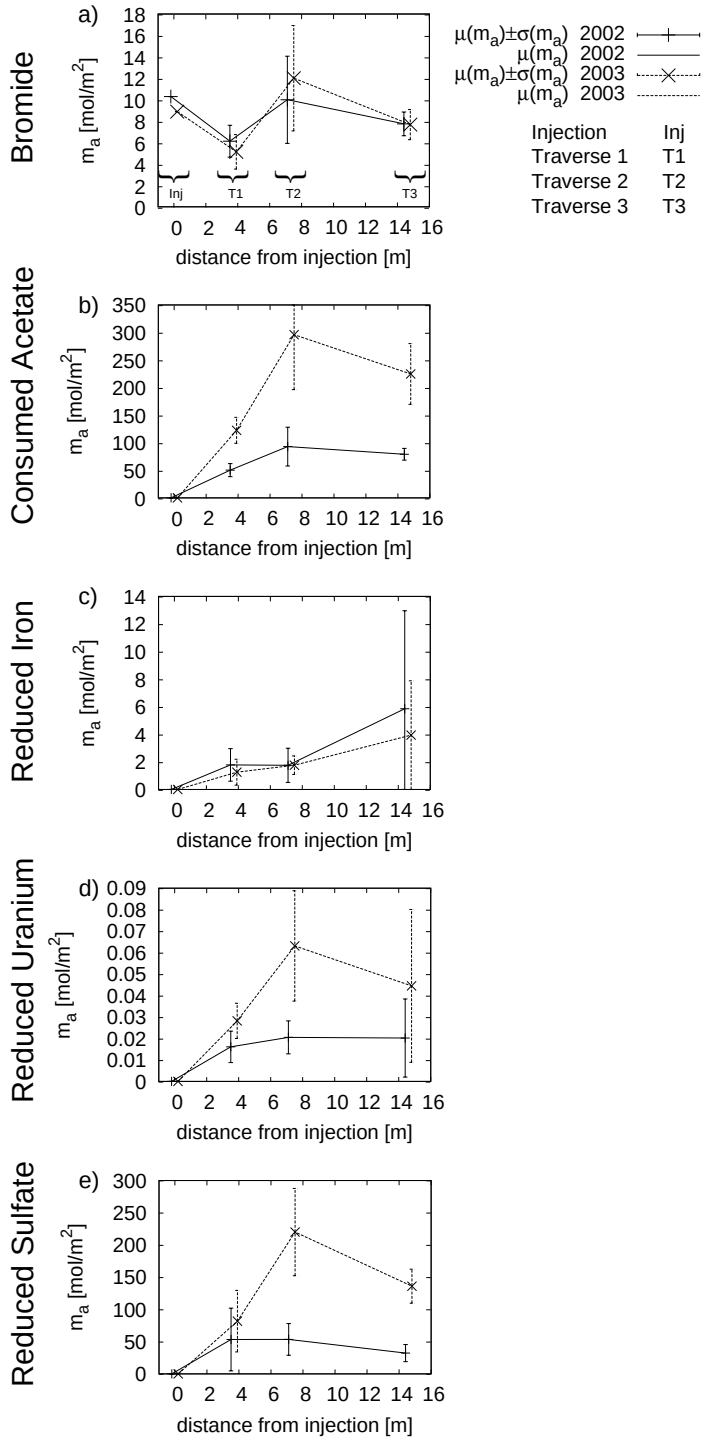

Figure 2: Statistics of the apparent accumulated mass (mean, $\mu(m_a)$, and standard deviation, $\sigma(m_a)$) of several species as a function of distance from the injection gallery, as obtained from the two experiments at the Rifle IFRC 2002/2003 site: Figure a shows statistics of m_a as an estimate of the injected and delivered amount of bromide to a given gallery or traverse (T#). Figure b shows the m_a statistics as an estimate of the amount of acetate consumed along the flowpaths to a given traverse. Figures c, d and e show statistics of m_a as an estimate of the amount of iron, uranium and sulfate reduced along the flowpaths to a given traverse. Traverses T1, T2 and T3 correspond to those indicated in Figure 1.

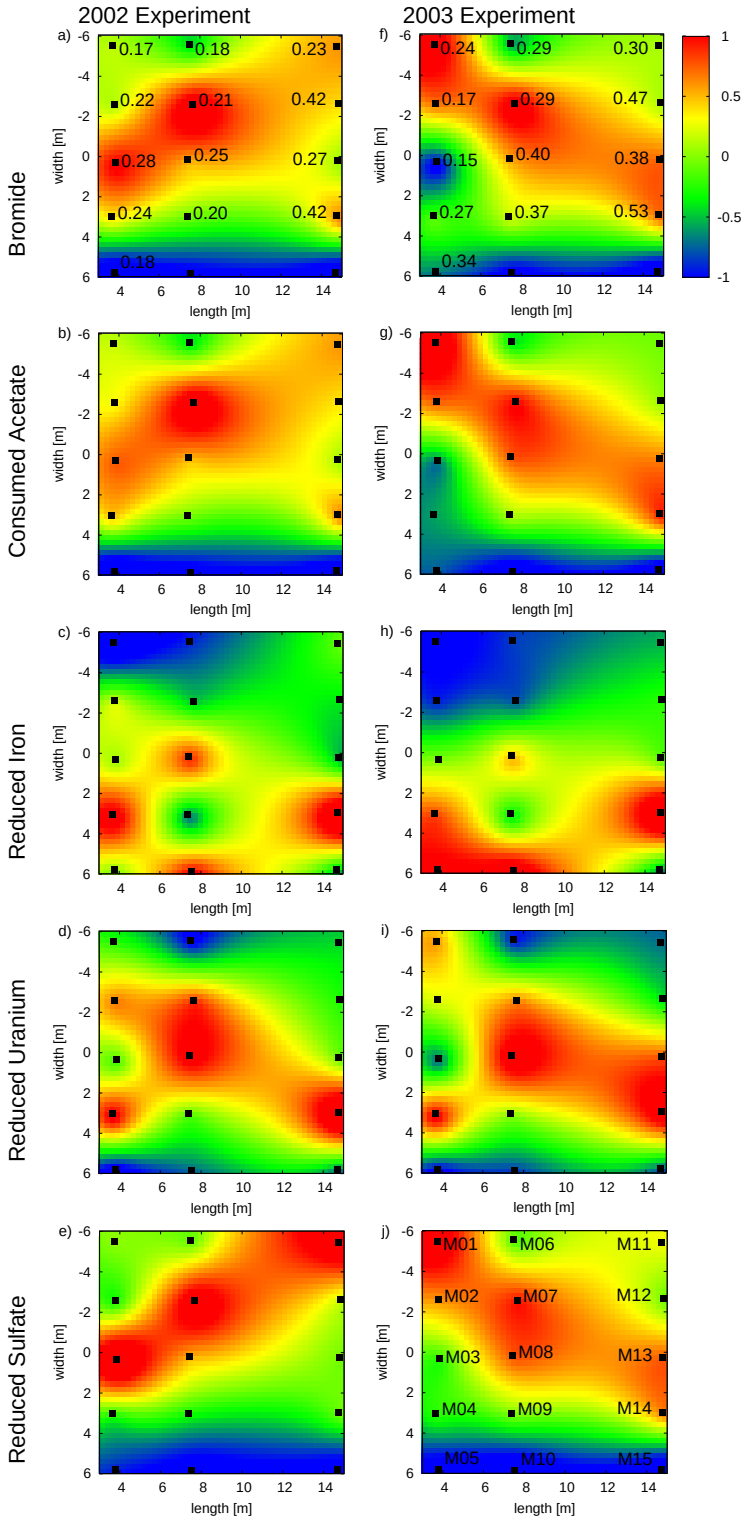

Figure 3: Contoured spatial patterns of the normalized apparent mass (m_a) of bromide (a and f), consumed acetate (b and g), reduced iron (c and h), uranium (d and i) and sulfate (e and j) during the 2002 (left) and 2003 (right) biostimulation experiments. As result of the normalization, the color-bar is a measure of the standard deviation from the mean values and is dimensionless. The Figures encompass the area in Figure 1 that includes the 15 downgradient monitoring wells. Superimposed on the patterns of the normalized m_a of bromide (a and f), are the apparent velocities in m/d. The monitoring well names are superimposed on Figure j.

Figures 3a and f show that significant differences (r=0.23) in the spatial patterns of the m_a^{norm} of bromide exist between the two experiments. Distributions of the m_a^{norm} of bromide generally coincide with the v_a distributions, whose values can vary by a factor two. Both the m_a^{norm} of bromide and the v_a show significant differences in their spatial patterns between the two experiments, indicating changes of the conservative transport behavior. Although different (r=0.37) between the two experiments, the spatial patterns of the m_a^{norm} of consumed acetate and the m_a^{norm} of bromide are similar ($0.96 \leq r \leq 0.99$) in both experiments (Figures 3a,b,f and g). This was to be expected and shows that the consumption of acetate is strongly governed by conservative transport processes.

Figures 3c and h reveal that the patterns of the m_a^{norm} of the reduced iron during the 2002 and 2003 experiment are similar (r=0.80). The dissimilarity ($0.00 \leq r \leq 0.38$) between the patterns of the m_a^{norm} of consumed acetate and of the reduced iron in both experiments suggests the influence of the acetate delivery on the patterns of the iron reduction to be minor (Figure 3b,c,g and h). This indicates that the intensity of the iron reduction is possibly governed by other factors, including geochemical heterogeneities (i.e., the distribution of "bioavailable" Fe(III) in the subsurface sediments). This observation is consistent with previous synthetic studies (*2*). Figures 3e and f reveal significant differences (r=0.26) in patterns of the m_a^{norm} of reduced sulfate between the 2002 and 2003 experiments, as was also observed for the m_a^{norm} of bromide and consumed acetate. However, the patterns of m_a^{norm} of reduced sulfate are similar ($0.68 \leq r \leq 0.90$) to those of bromide and consumed acetate. These observations indicate that the intensity of the sulfate reduction is dominated by the delivery of acetate, which in turn is governed by conservative transport processes. Inspection of the patterns of the m_a^{norm} of reduced uranium indicates that the uranium reduction patterns were similar (r=0.87) for both experiments (Figure 3d and i). During the low acetate delivery in the 2002 experiment, the patterns of the m_a^{norm} of reduced uranium coincided (r=0.73) with those of the m_a^{norm} of reduced iron (Figure 3c and d). During high acetate delivery in the 2003 experiment, the patterns of the m_a^{norm} of reduced uranium coincided (r=0.80) with those of the m_a^{norm} of bromide (Figure 3f and i). This suggests that iron geochemistry may predominantly govern uranium reduction under low acetate conditions whereas hydrological heterogeneity may dominate during the high acetate conditions.

Discussion

We used a temporal moment analysis that relies on a streamtube approximation to characterize apparent velocity and masses of conservative and reactive species during two sequential biostimulation experiments. The apparent mass permitted integration over the time of an experiment and thus quantification of the accumulated responses (i.e., the iron, uranium and sulfate reduction) of a subsurface system as a function of the introduced species (i.e., acetate and bromide). A benefit of the measure of the apparent mass is that no assumptions need to be made about the reaction kinetics during the estimation, while a limitation is that the temporal dynamics of the chemical reactions are lost due to the integration over time. The apparent mass provides spatial information about the status of the overall reactive transport in the direction of flow and about the relation between the hydrological and geochemical heterogeneity and the conservative and reactive transport processes in a direction perpendicular to the mean flow. The apparent masses of consecutive experiments provide temporal information about changes in the subsurface system.

Application of the developed approach to the two biostimulation experiments suggests that sulfate reduction was dominated by the hydrological heterogeneity and that the iron reduction was dominated by the geochemical heterogeneity of the subsurface. Uranium reduction showed variable behavior as a function of acetate injection. During relatively low acetate concentrations (2002 experiment), our results indicate that the uranium reduction was dominated by the geochemical heterogeneity, as the spatial distribution of the apparent mass was similar to the one of the iron reduction. During prolonged acetate injection (2003 experiment), our results indicated the uranium reduction was dominated by the hydrological heterogeneity, as was the sulfate reduction.

Significant changes in the apparent velocities and the apparent masses of bromide between the 2002 and 2003 experiments suggested that the hydrology of the system was modified as a result of the biostimulation experiment, perhaps due to clogging associated with the formation of biofilms, bioaggregates, and precipitates. Our interpretation is supported by ongoing reactive transport modeling of the Rifle IFRC biostimulation experiments that include the evolution of precipitates and biomass (*14*). This ongoing research suggests that the evolution of biomass, FeS, and calcite can lead to accumulations that may be sufficient to block pore throats and thus to alter flow

characteristics.

Our study has shown that a temporal moment approach permits the quantification of the spatial and temporal distributions of the intensity of amendment delivery and of reactions and their relations to conservative transport characteristics. Through assessment of the spatial patterns of the flow and the apparent mass, new insights about the influence of hydrological and biogeochemical heterogeneity on the biostimulation experiments and their changes over time were developed. In particular, we illustrated that feedbacks between hydrological heterogeneity and bioremediation-induced biogeochemical transformations exist at the field scale. In addition to potentially impacting the efficacy and sustainability of contaminant remediation, such feedbacks could play an important role in other subsurface manipulations, such as enhanced oil recovery or carbon dioxide sequestration.

Acknowledgment

Funding for this study was provided by the Environmental Remediation Science Program, Office of Biological and Environmental Research, U.S. Department of Energy (DOE Grant DE-AC02-05CH11231) as part of the LBNL Sustainable Systems Science Focus Area. We sincerely thank Dr. Philip Long (PNNL) and the DOE Rifle, CO Integrated Field Research Center team for allowing us to work with their historical dataset. We thank Dr. Steven Yabusaki (PNNL) for many fruitful discussions about hydrological gradients and dataset nuances associated with the study site. We thank the three anonymous reviewers.

Supporting Information Available

This information is available free of charge via the Internet at http://pubs.acs.org.

References

(1) Lovley, D. R. Cleaning up with genomics: Applying molecular biology to bioremediation. *Nature Reviews Microbiology* **2003**, *1*, 35–44, 10.1038/nrmicro731.

(2) Scheibe, T. D.; Fang, Y.; Murray, C. J.; Roden, E. E.; Chen, J.; Chien, Y.-J.; Brooks, S. C.; Hubbard, S. S. Transport and biogeochemical reaction of metals in a physically and chemically heterogeneous aquifer. *Geosphere* **2006**, *2*, 220–235.

(3) Hubbard, S.; Williams, K.; Conrad, M.; Faybishenko, B.; Peterson, J.; Chen, J.; Long, P.; Hazen, T. Geophysical monitoring of hydrological and biogeochemical transformations associated with Cr(VI) bioremediation. *Environmental Science & Technology* **2008**, *42*, 3757–3765, 10.1021/es071702s.

(4) Baveye, P.; Vandevivere, P.; Hoyle, B.; DeLeo, P.; de Lozada, D. Environmental impact and mechanisms of the biological clogging of saturated soils and aquifer materials. *Critical Reviews in Environmental Science and Technology* **1998**, *28*, 123–191.

(5) Thullner, M.; Mauclaire, L.; Schroth, M. H.; Kinzelbach, W.; Zeyer, J. Interaction between water flow and spatial distribution of microbial growth in a two-dimensional flow field in saturated porous media. *Journal Of Contaminant Hydrology* **2002**, *58*, 169–189.

(6) Seifert, D.; Engesgaard, P. Use of tracer tests to investigate changes in flow and transport properties due to bioclogging of porous media. *Journal Of Contaminant Hydrology* **2007**, *93*, 58–71.

(7) Kapellos, G. E.; Alexiou, T. S.; Payatakes, A. C. Hierarchical simulator of biofilm growth and dynamics in granular porous materials. *Advances In Water Resources* **2007**, *30*, 1648–1667.

(8) Seymour, J. D.; Gage, J. P.; Codd, S. L.; Gerlach, R. Magnetic resonance microscopy of biofouling induced scale dependent transport in porous media. *Advances In Water Resources* **2007**, *30*, 1408–1420.

(9) Wu, W. M.; Carley, J.; Fienen, M.; Mehlhorn, T.; Lowe, K.; Nyman, J.; Luo, J.; Gentile, M. E.; Rajan, R.; Wagner, D.; Hickey, R. F.; Gu, B. H.; Watson, D.; Cirpka, O. A.; Kitanidis, P. K.; Jardine, P. M.; Criddle, C. S. Pilot-scale in situ bioremediation of uranium in a highly contaminated aquifer. 1. Conditioning of a treatment zone. *Environmental Science & Technology* **2006**, *40*, 3978–3985.

(10) Faybishenko, B.; Hazen, T. C.; Long, P. E.; Brodie, E. L.; Conrad, M. E.; Hubbard, S. S.; Christensen, J. N.; Joyner, D.; Borglin, S. E.; Chakraborty, R.; Williams, K. H.; Peterson, J. E.; Chen, J.; Brown, S. T.; Tokunaga, T. K.; Wan, J.; Firestone, M.; Newcomer, D. R.; Resch, C. T.; Cantrell, K. J.; Willett, A.; Koenigsberg, S. In Situ Long-Term Reductive Bioimmobilization of Cr(VI) in Groundwater Using Hydrogen Release Compound. *Environmental Science & Technology* **2008**, accepted.

(11) Anderson, R. T.; Vrionis, H. A.; Ortiz-Bernad, I.; Resch, C. T.; Long, P. E.; Dayvault, R.; Karp, K.; Marutzky, S.; Metzler, D. R.; Peacock, A.; White, D. C.; Lowe, M.; Lovley, D. R. Stimulating the in situ activity of Geobacter species to remove uranium from the groundwater of a uranium-contaminated aquifer. *Applied And Environmental Microbiology* **2003**, *69*, 5884–5891.

(12) Vrionis, H. A.; Anderson, R. T.; Ortiz-Bernad, I.; O'Neill, K. R.; Resch, C. T.; Peacock, A. D.; Dayvault, R.; White, D. C.; Long, P. E.; Lovley, D. R. Microbiological and geochemical heterogeneity in an in situ uranium bioremediation field site. *Applied And Environmental Microbiology* **2005**, *71*, 6308–6318.

(13) Yabusaki, S. B.; Fang, Y.; Long, P. E.; Resch, C. T.; Peacock, A. D.; Komlos, J.; Jaffe, P. R.; Morrison, S. J.; Dayvault, R. D.; White, D. C.; Anderson, R. T. Uranium removal from groundwater via in situ biostimulation: Field-scale modeling of transport and biological processes. *Journal Of Contaminant Hydrology* **2007**, *93*, 216–235.

(14) Li, L.; Steefel, C. I.; Kowalsky, M. B. Biogeochemical Reaction Kinetics Associated With Uranium Bioremediation at Multiple Scales. *Eos Trans. AGU, Fall Meet. Suppl.*, 2007; pp H32D–03.

(15) Kreft, A.; Zuber, A. Physical Meaning Of Dispersion-Equation And Its Solutions For Different Initial And Boundary-Conditions. *Chemical Engineering Science* **1978**, *33*, 1471–1480.

(16) Harvey, C. F.; Gorelick, S. M. Temporal Moment-Generating Equations - Modeling Transport And Mass-Transfer In Heterogeneous Aquifers. *Water Resources Research* **1995**, *31*, 1895–1911.

(17) Vanderborght, J.; Vereecken, H. Analyses Of Locally Measured Bromide Breakthrough Curves From A Natural Gradient Tracer Experiment At Krauthausen. *Journal Of Contaminant Hydrology* **2001**, *48*, 23–43.

(18) Jose, S. C.; Rahman, M. A.; Cirpka, O. A. Large-Scale Sandbox Experiment On Longitudinal Effective Dispersion In Heterogeneous Porous Media. *Water Resources Research* **2004**, *40*, W12415.

(19) Dagan, G.; Cvetkovic, V.; Shapiro, A. A Solute Flux Approach To Transport In Heterogeneous Formations .1. The General Framework. *Water Resources Research* **1992**, *28*, 1369–1376.

(20) Cvetkovic, V.; Shapiro, A. M.; Dagan, G. A Solute Flux Approach To Transport In Heterogeneous Formations .2. Uncertainty Analysis. *Water Resources Research* **1992**, *28*, 1377–1388.

(21) Cirpka, O. A.; Kitanidis, P. K. Characterization Of Mixing And Dilution In Heterogeneous Aquifers By Means Of Local Temporal Moments. *Water Resources Research* **2000**, *36*, 1221–1236.

(22) Vanderborght, J.; Kemna, A.; Hardelauf, H.; Vereecken, H. Potential of electrical resistivity tomography to infer aquifer transport characteristics from tracer studies: A synthetic case study. *Water Resources Research* **2005**, *41*, W06013, doi:10.1029/2004WR003774.

(23) Bloem, E.; Vanderborght, J.; de Rooij, G. Leaching surfaces to characterize transport in a heterogeneous aquifer: Comparison between flux concentrations, resident concentrations, and flux concentrations estimated from temporal moment analysis. *Water Resources Research* **2008**, *44*, W10412, doi:10.1029/2007WR006425.

Supporting Information

Feedbacks Between Hydrological Heterogeneity and Bioremediation Induced Biogeochemical Transformations

A. Englert[12], S.S. Hubbard[1], K.H. Williams[1], L. Li[1], C.I. Steefel[1]

[1]Earth Sciences Division, Lawrence Berkeley National Laboratory

[2]now at Bochum University, Applied Geology Department

April 25, 2009

In the following the supporting information are organized as follows:

Materials and Methods

Temporal Moment Analysis and Apparent Velocity Estimation

Hydraulic Gradients During the Biostimulation Experiments

Estimation of the Injection Function

Biogeochemical Network

Results

Correlation of Apparent Masses of Reactive and non Reactive Species

Statistical Tests

Materials and Methods

Temporal Moment Analysis and Apparent Velocity Estimation

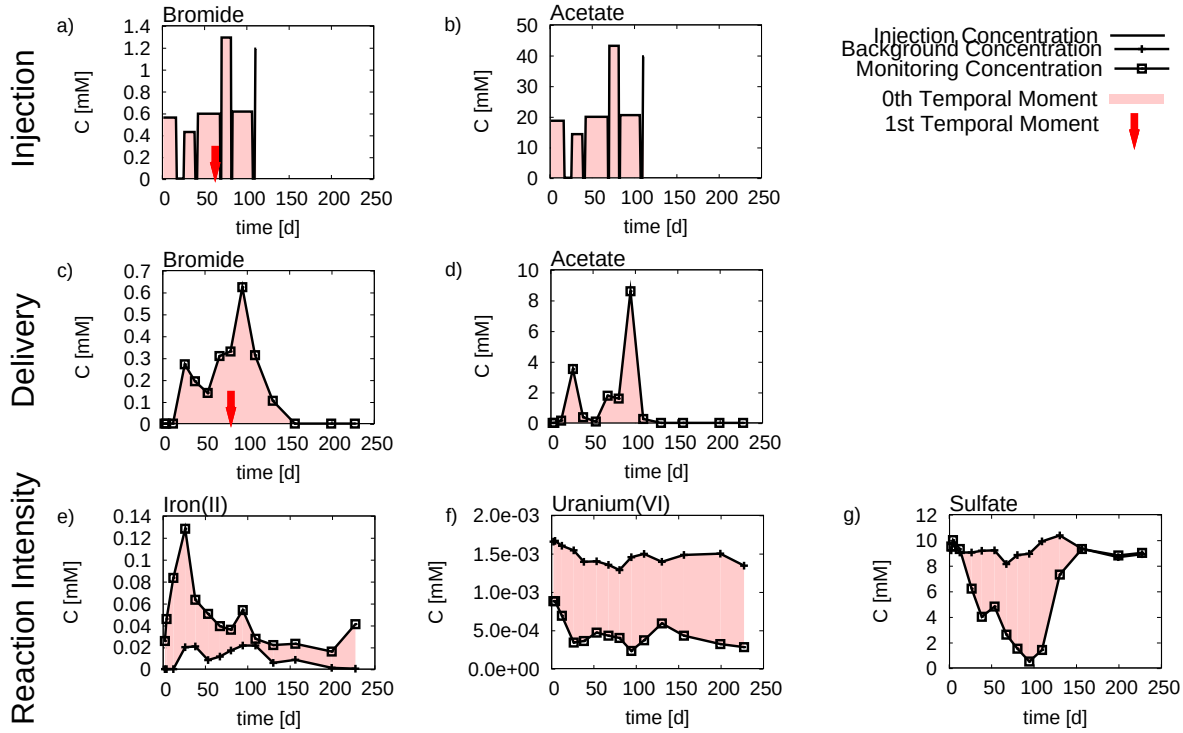

Figure SI-1: Selected time-lapse concentration data acquired during the 2003 biostimulation experiment at the Rifle IFRC site (Figure 1). Figures a-b show the average bromide and acetate concentrations introduced via the injection gallery. Figures c-g show the time lapse concentrations of several species measured at monitoring well M08. Figures e-f show also the time lapse average concentration measured at the three background wells. The part of the graphs highlighted in light red shading is the area that, upon integration, yields the zeroth temporal moment. The first temporal moment for the bromide injection and breakthrough is indicated by a red arrow in Figure a and c.

Hydraulic Gradients During the Biostimulation Experiments

The flow velocity field during field experiments impacts the advective component of the reactive transport process. The flow velocity field is a result of the heterogeneity of the hydraulic conductivity and the magnitude and direction of the mean hydraulic gradient. For the application of the proposed procedures to estimate the apparent velocity and mass, variations of the mean gradient should be small. Furthermore, for comparing the two experiments (2002 and 2003) in terms of the apparent mass, the magnitude of the mean gradient and it's direction should be similar in both experiments. In the following, we examine the variability of the magnitude of the mean gradient and it's direction for both experiments. Thereto, we used multiple regression to fit planes to the measured groundwater levels. This procedure results into representation of the water level at a given location as a function of northing and easting of this location (water level=a·northing+b·easting). In Figure SI-2 the results of plane fitting are presented in comparison with linear interpolated groundwater level contour plots for the groundwater level measurements conducted at day 80 in both experiments.

Comparison of the interpolated and plane fitted groundwater level contourplots shows the effect of simplification through the plane fitting procedure in both experiments. As consequence, there are differences between the contourplots (visualized in Figure SI-2), which can be up to one centimeter. However, the resolution of the groundwater level measurements is of the same order of magnitude, in particular +-1 cm. Thus, it can not be distinguished in the interpolated plots, whether the complex shape of the contour lines are due to real spatial variability of groundwater levels or due to measurement errors. To minimize the influence of artifacts from measurement errors during the estimation of mean gradients and mean directions, the plane fitting results are utilized in the following to assess the variability of gradient and direction with time.

The plane fitting procedure results in estimates of coefficients in northing (a) and easting (b) and a "standard error of estimate" of these coefficients. The coefficients a and b represent the components of the mean hydraulic gradient in northing and easting direction. Using Pythagorean theorem we estimated the hydraulic gradient magnitude and its standard error based on the prior estimated components a and b and their standard errors. For every time groundwater levels were

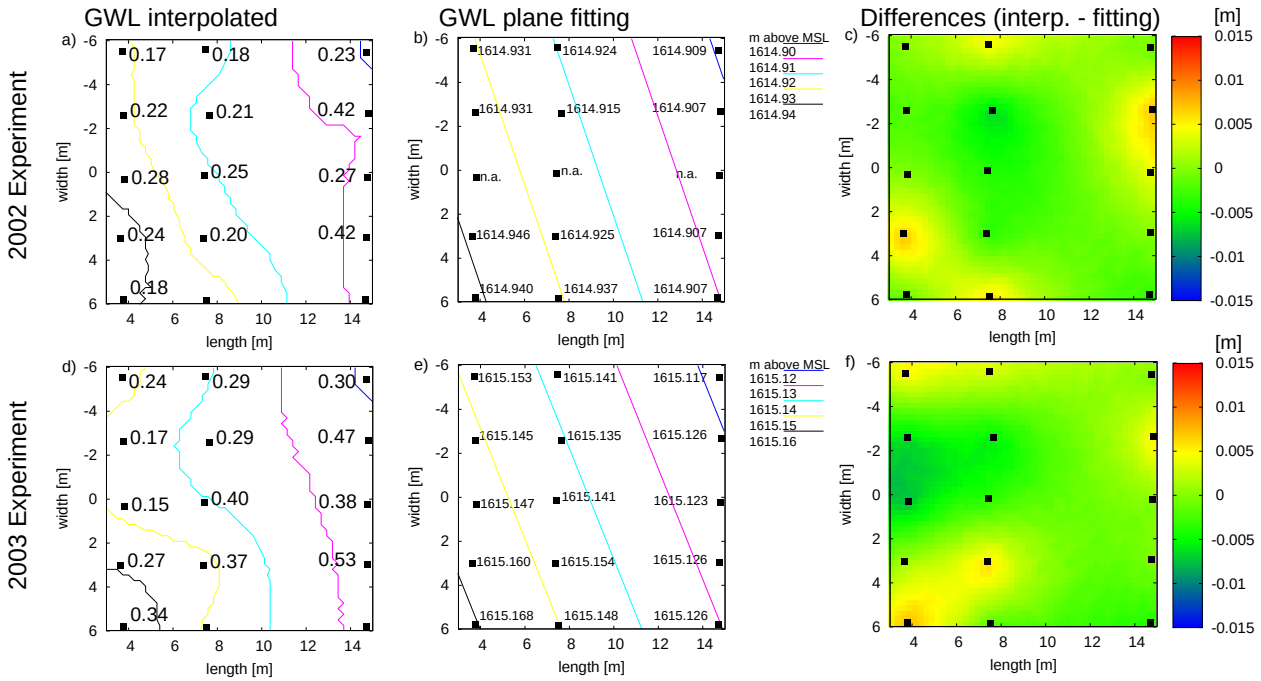

Figure SI-2: Groundwater level contour plots based on linear interpolation and plane fitting using groundwater level measurements of day 80 at the Rifle site (highlighted superimposed on Figure b and e): Linear interpolated contour plots of the groundwater levels are shown Figure a and b. Apparent velocities (m/d) are shown superimposed on Figure a and b. Contour plots as result of plane fitting are shown in Figure b and e. The differences between the interpolated and plane fitted contour plots are shown in Figure c and f. Although the precision of the groundwater level measurements is +-1 cm, we included three digits after decimal point to avoid artifacts from conversion foot to meter.

available during the experiments the estimate of the magnitude (+ in 2002 and x in 2003) together with it's standard error (vertical errorbars attached to + and x) are shown in Figure SI-3. The estimated coefficients (a and b) and their standard errors are subsequently utilized to estimate an average of the coefficients and standard errors for both experiments. Using again Pythagorean theorem we estimated the average hydraulic gradient magnitude and its average standard error based on the prior estimated average components a and b and their average standard errors. The average of the mean gradients and their average standard errors are highlighted in horizontal lines in Figure SI-3.

Using trigonometry, the coefficients and their standard errors from plain fitting were used to estimate the direction (deviation from the length axis of the experiments in degrees) of the hydraulic gradient and the standard errors thereof. For every time during the experiment, where groundwater

levels were measured this procedure was performed and the resulting deviations from the length axis of the experiment are visualized together with their standard errors in Figure SI-4. There, deviations in degrees are highlighted in "+" for the 2002 and in "x" for the 2003 experiment. The approximated standard error of the deviations are attached to "+" and "x" as vertical error bars. The average of the estimated coefficients (a and b) and their standard errors are subsequently utilized to estimate an average direction and standard error for both experiments. The average direction and its standard error is highlighted for both experiments as horizontal lines in Figure SI-4.

Although the estimation of the magnitude (Figure SI-3) and the direction (Figure SI-4) of the hydraulic gradient is connected with distinct uncertainties, the integrated analysis of all available groundwater level measurements show only slight deviation from the direction of the long axis of the experimental layout and a fairly constant magnitude of the hydraulic gradient. More important, the magnitude and direction of the hydraulic gradient are similar in both experiments. Motivated by these observations, we assumed that changes in apparent parameters observed in the study are only marginally influenced by changes in the mean gradient but primarily impacted by changes in the physico-chemical heterogeneity of the subsurface.

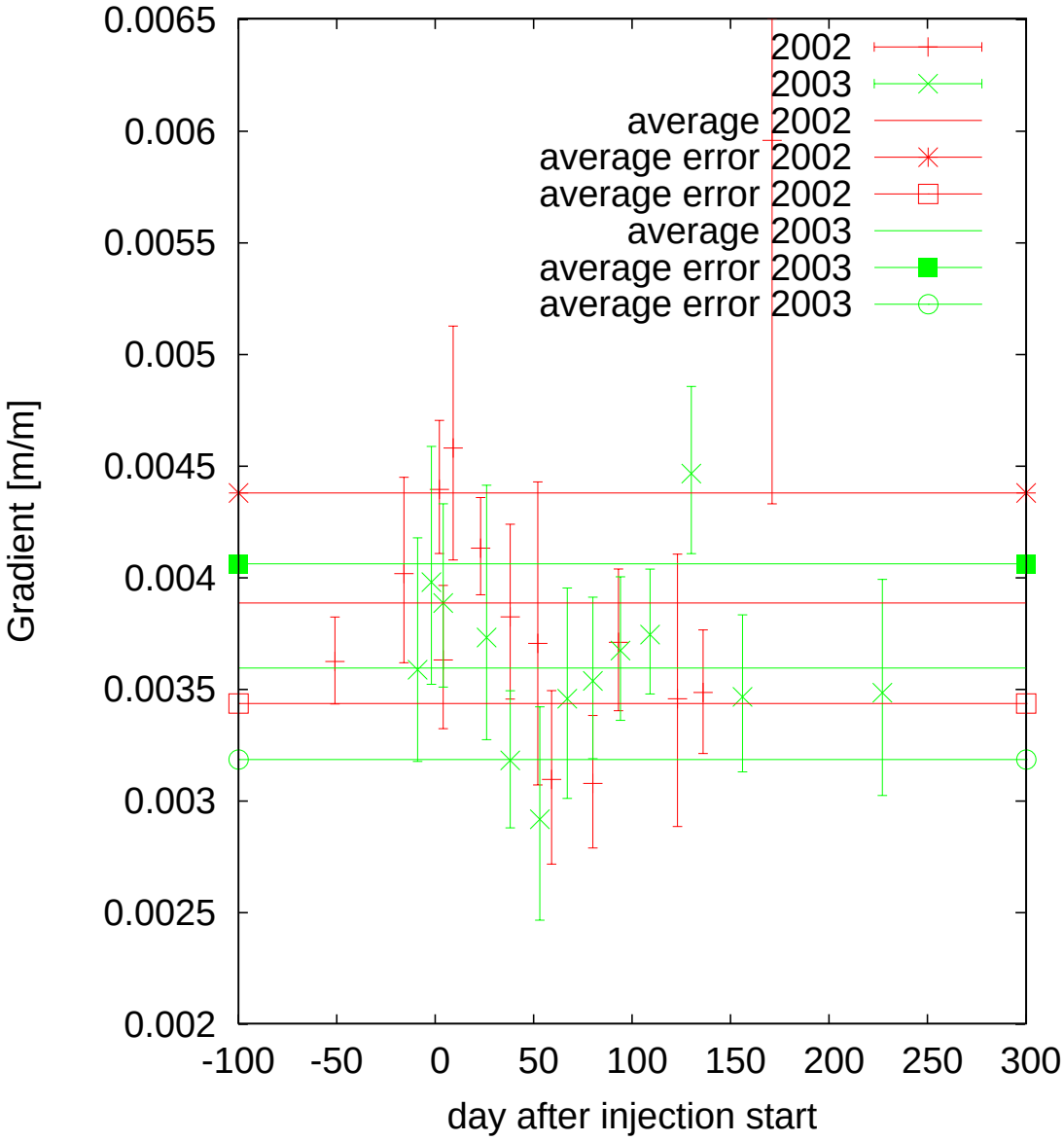

Figure SI-3: Variability and uncertainty of the mean hydraulic gradient as a function of time during the 2002 and 2003 biostimulation experiments.

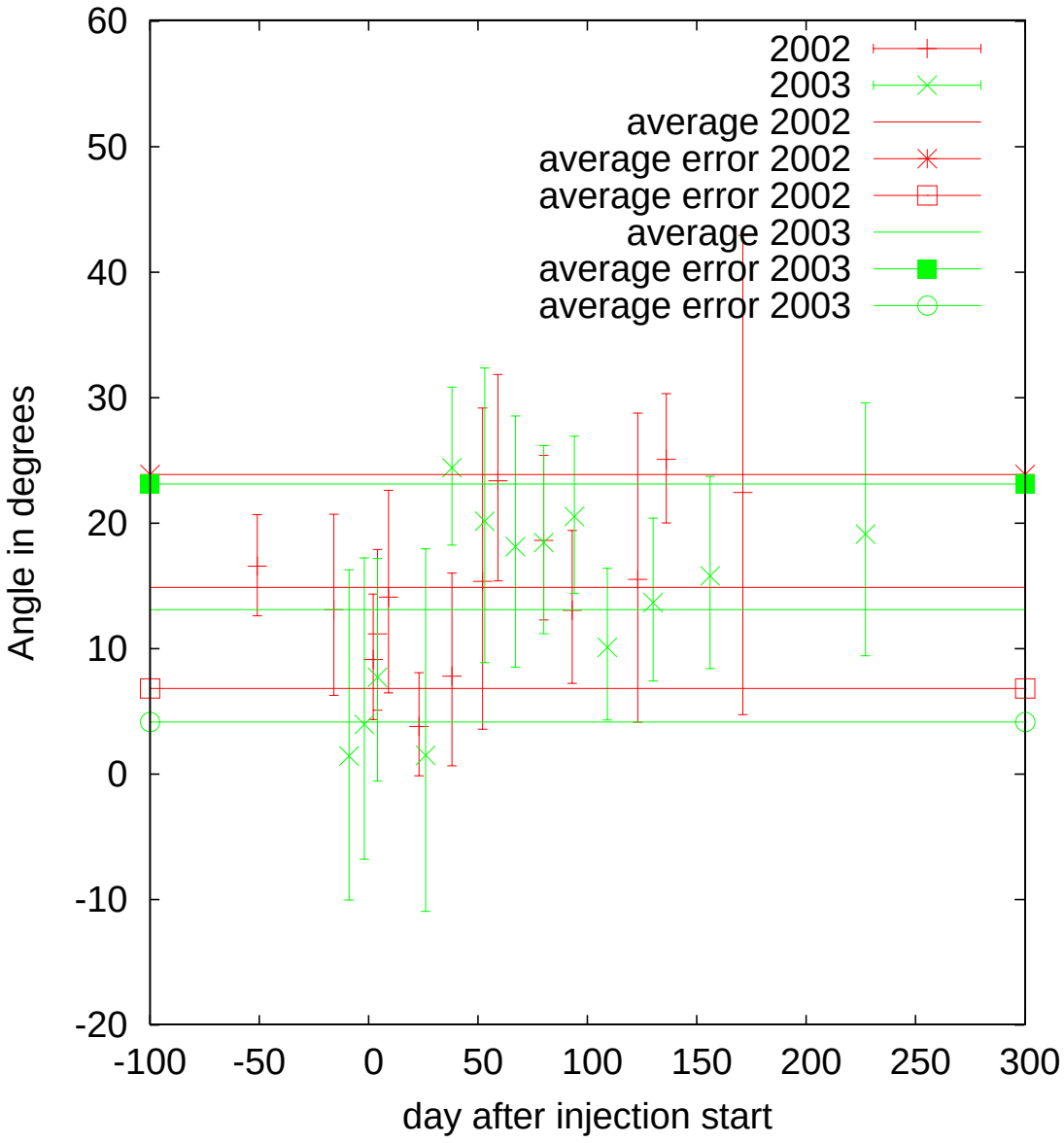

Figure SI-4: Variability and uncertainty of the deviation of the direction of the mean hydraulic gradient as a function of time during the 2002 and 2003 biostimulation experiments. With a view from the injection gallery in direction monitoring wells, positive angles indicate a deviation to the left of the alignment of the experimental layout (Figure 1), negative angles to the right.

Estimation of the Injection Function

To estimate the apparent velocity and mass at monitoring wells, an estimation of the zeroth and first temporal moment of the injection function of bromide is required. The injection function of bromide at the two Rifle experiments can be estimated, based on field observations as follows: Measurements of the concentrations of bromide in the tank were utilized together with measurements of tank levels and dimensions of the tank to infer an approximated concentration of bromide (Figure SI-5a) in the tank and a flow rate of the injection as function of time (Figure SI-5b). The measurements of groundwater levels in the vicinity of the injection gallery were utilized together with the width of the injection gallery to estimate the saturated area covered by the injection gallery as function of time (not shown). Based on Darcy law the saturated area of the injection gallery together with the mean hydraulic conductivity of the site and the mean hydraulic gradient during an experiment the flow through the injection gallery can be estimated as a function of time (Figure SI-5b). Assuming complete mixing between the injected water and the water which flows through the injection gallery an average injection function can be estimated using

$$C_{injection}(t) = \frac{C_{tank}(t)Q_{injection}(t)}{Q_{injection}(t) + Q_{gallery}(t)}, \tag{1}$$

where $C_{injection}(t)$ is the estimated concentration in the vicinity of the injection gallery, $C_{tank}(t)$ is the concentration in the tank, $Q_{injection}(t)$ is the flow rate from the tank into the injection gallery, and $Q_{gallery}(t)$ is the natural flow through the injection gallery. The injection function, estimated based on Equation 1, is shown for the 2003 experiment in Figure SI-5c.

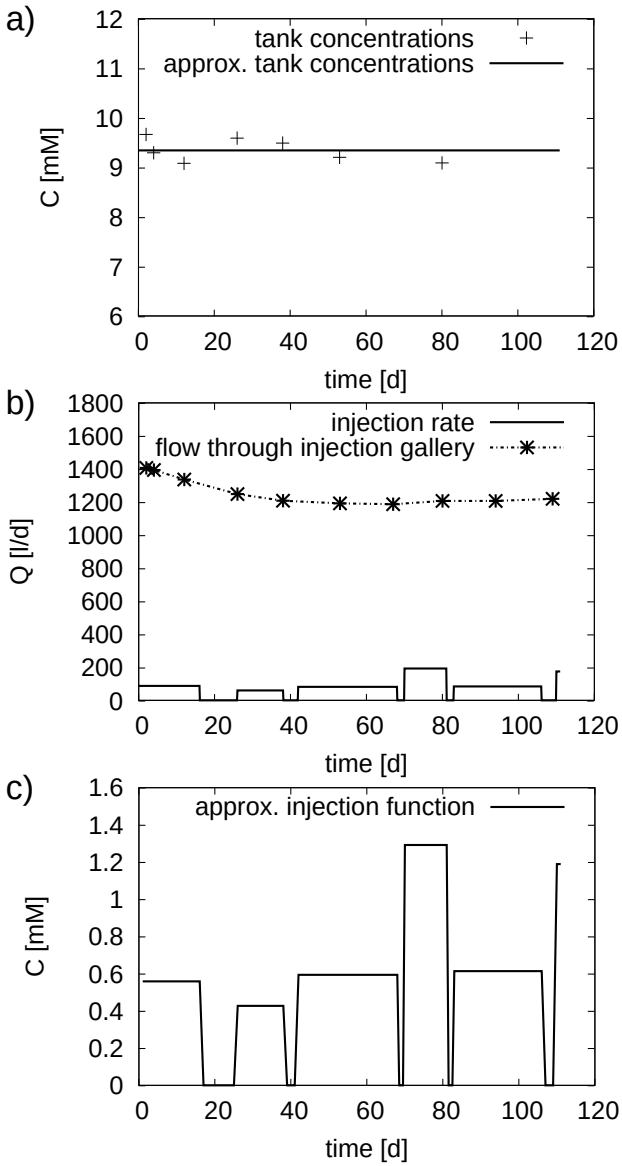

Figure SI-5: Estimation of the injection function for the 2003 experiment at the Rifle site.

Biogeochemical Network

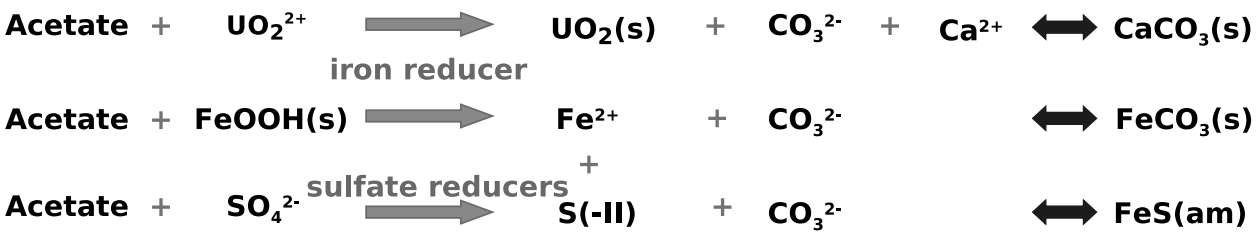

Figure SI-6: Schematic reaction network of the 2002/2003 Rifle IFRC biostimulation experiments.

Results

Correlation of Apparent Masses of Reactive and non Reactive Species

To augment the plots, shown in Figure 3, which facilitate visual assessment only, we present the correlation matrix of different species' m_a as shown in Table SI-1.

Table SI-1: Correlation Matrix of Traverse-wise Normalized Apparent Accumulated Mass

		Bromide		Acetate Cons.		Red. Iron		Red. Uranium		Red. Sulfate	
		2002	2003	2002	2003	2002	2003	2002	2003	2002	2003
Bromide	2002	1	0.23	0.99	0.32	0.36	-0.02	0.65	0.35	0.73	0.42
	2003	0.23	1	0.30	0.96	0.06	-0.05	0.60	0.80	-0.08	0.89
Cons.	2002	0.99	0.30	1	0.37	0.38	-0.04	0.70	0.42	0.68	0.47
Acetate	2003	0.32	0.96	0.37	1	0.11	0.00	0.62	0.76	-0.01	0.90
Red.	2002	0.36	0.06	0.38	0.11	1	0.80	0.73	0.5	-0.01	0.09
Iron	2003	-0.02	-0.05	-0.04	0.00	0.80	1	0.38	0.33	-0.27	-0.12
Red.	2002	0.65	0.60	0.70	0.62	0.73	0.38	1	0.87	0.10	0.61
Uranium	2003	0.35	0.80	0.42	0.76	0.5	0.33	0.87	1	-0.10	0.77
Red.	2002	0.73	-0.08	0.68	-0.01	-0.01	-0.27	0.10	-0.10	1	0.26
Sulfate	2003	0.42	0.89	0.47	0.90	0.09	-0.12	0.61	0.77	0.26	1

Statistical Tests

To quantitatively back up the discussion on the development of the statistics of the apparent mass with distance to the injection gallery (Figure 2), we performed statistical tests. For comparison of averages we performed "Welch tests" including a null hypothesis that the averages are equal, and a confidence level of 0.95. For comparing standard deviations we performed "F tests" including a null hypothesis that the standard deviations are equal, and a confidence level of 0.95. Results of the testing are presented in Tables SI-2-SI-3. Probabilities $\leq$0.05 indicate the compared averages or standard deviations are significantly different, probabilities $\geq$0.95 indicate that compared averages or standard deviations are equal. In Table SI-2 the averages and standard deviations of the 2002 experiment are compared to those of the 2003 experiment for every species and traverse. In Table SI-3 the averages and standard deviations of neighboring traverses are compared for every species in both experiments.

Table SI-2: "Welch Test" and "F Test" results of apparent mass statistics being equal in 2002 and 2003 (probability of the null hypothesis)

	first		second		third	
	$\mu(m_a)$	$\sigma(m_a)$	$\mu(m_a)$	$\sigma(m_a)$	$\mu(m_a)$	$\sigma(m_a)$
Bromide	0.3347	0.881	0.5613	0.7641	0.9296	0.7033
Consumed Acetate	0.03658	2.098e-05	0.06709	0.0001	0.03049	3.149e-05
Reduced Iron	0.4539	0.6659	0.9866	0.3363	0.66	0.3579
Reduced Uranium	0.03997	0.8297	0.04008	0.07725	0.2843	0.2973
Reduced Sulfate	0.3783	0.9681	0.01132	0.1303	0.001499	0.2854

Table SI-3: "Welch Test" and "F Test" results of apparent mass statistics being equal in neighboring traverses (probability of the null hypothesis)

	first-second		second-third	
	$\mu(m_a)$	$\sigma(m_a)$	$\mu(m_a)$	$\sigma(m_a)$
Bromide in 2002	0.1499	0.08119	0.3513	0.06008
Bromide in 2003	0.06317	0.0563	0.1768	0.06912
Consumed Acetate in 2002	0.6256	0.3826	0.07439	0.01207
Consumed Acetate in 2003	0.2201	0.1513	0.1357	0.03659
Reduced Iron in 2002	0.9653	0.8924	0.3339	0.01716
Reduced Iron in 2003	0.3750	0.6021	0.3502	0.01580
Reduced Uranium in 2002	0.4209	0.893	0.9775	0.1910
Reduced Uranium in 2003	0.06825	0.05131	0.432	0.6066
Reduced Sulfate in 2002	0.9963	0.2911	0.1936	0.334
Reduced Sulfate in 2003	0.01695	0.5074	0.0832	0.1558